**Proceedings of the ASME 2023 International Technical Conference and Exhibition on Packaging and Integration of Electronic and Photonic Microsystems**
**InterPACK2023**
**October 24-26, 2023, San Diego, California**

**IPACK2023-112452**



# EXPERIMENTAL AND NUMERICAL INVESTIGATION OF SINGLE-PHASE LIQUID COOLING FOR HETEROGENEOUS INTEGRATION MULTI-CHIP MODULE

**Ahmad R Gharaibeh**
Binghamton University
Binghamton, NY

**Qusai Soud**
Binghamton University
Binghamton, NY

**Yaman Manaserh**
Binghamton University
Binghamton, NY

**Mohammed Tradat**
Binghamton University
Binghamton, NY

**Bahgat Sammakia**
Binghamton University
Binghamton, NY

## ABSTRACT

*The variety of new electronic packaging technologies has grown significantly over the last 20 years as a result of market demands for higher device performance at lower costs and in less space. Those demands have pushed for heterogeneous packaging, where computer chips with different stack heights are closely packed, creating non-uniform multicore chip heat flux and temperature and additional challenges for thermal management. Without implementing an appropriate thermal management strategy for heterogeneous packages, large temperature gradients can be observed within the package, which would increase the thermal stresses on the chip and raise reliability issues. Therefore, removing excessive heat flux will improve the reliability and efficiency of those electronic components. The development of high-heat flux applications is straining the capabilities of air-cooling systems, which are nearing their limitations. Single-phase liquid cooling methods have proven to be reliable, usable, and energy-efficient methods for cooling high-heat flux devices. With the introduction of packages with multiple-chip modules (MCMs), the cold plates of future generations are expected to handle multiple hot spots at the same time. To enable the effective removal of heat from the chips, special cold plate designs for each type of package are required. Many methods may be used to improve thermohydraulic performance, including the use of improved fin designs, flow restriction to breakdown the boundary layer, and the integration of mixing mechanisms to improve the mixing between the fluid and channel walls. To mimic this real-life scenario of such packaging in high-heat flux applications, an experimental setup was designed and built. The design of the new experimental setup consists of four identical 1.2 cm × 1.2 cm ceramic heaters, each of which is connected to a separate power supply and can reach a heat flux of 140 W/cm$^2$. Accordingly, this mock package is capable of delivering different power levels to mimic different multicore microprocessor conditions. To give the heater the ability to move precisely in the x, y, and z directions with high precision, each heater is mounted to an XYZ linear stage. Deionized water (DI) was used as the working fluid, and a commercially available pin-fin heat sink was used to run the initial steady-state tests on the experimental rig. The tests showed how different flow rates at a constant fluid temperature and input power affect the temperatures of the heaters and the thermohydraulic performance of the heat sink. In addition, a three-dimensional numerical model has been developed and validated with experimental data in terms of heat sink pressure drop and temperatures of the heaters.*

Keywords: Multi-chip module, Liquid cooling, Heat sink, Data centers, Heat transfer.

## 1. INTRODUCTION

The world is being inundated with an overwhelming amount of digital data from numerous sources, including social media, blog posts, trading, artificial intelligence, quantum computing, and the Internet of Things. To accommodate and manage this overwhelming amount of data, data centers are required to capture, route, store, evaluate, and retrieve this massive amount of information, resulting in a rise in the energy they consume. An estimated 1.31% of the world's yearly energy consumption is utilized by data centers, with the cooling infrastructure responsible for up to half of that [1]–[3]. Enhancing the energy efficiency of power-hungry technologies in data centers is

therefore becoming more crucial. In addition, the development of chips along with additional integrated components, together with the expanding need for data processing, will increase the power density of chips and heat dissipation. Air-cooling solutions, which are the most popular cooling systems in data centers, have several limitations, including poor heat transfer coefficients, inefficient energy use, and high levels of noise [4]–[6]. Because of this, alternate cooling methods, including single-phase liquid cooling and two-phase cooling, have become more popular. According to research studies [7]–[10], the challenge of cooling high-heat flux devices can be accomplished by adopting single-phase on-chip liquid cooling systems, as they are efficient, practical, and reliable.

Advanced chips typically have several cores integrated into them to improve performance, which can lead to temperature nonuniformity. Without an efficient thermal management system, the package can encounter large temperature gradients, which impose more thermal stress on the chip. Bar-Cohen [11] covered liquid and air-cooling techniques for the thermal management of multichip modules (MCMs). The researcher investigated different approaches for enhancing heat transfer and lowering thermal resistance in MCMs, including the utilization of thermally conductive adhesives and the design of innovative heat sinks. Ansari [12] developed a hybrid heat sink with pin-fins and microchannels to cool microprocessors with uneven power dispersions. Compared with traditional heat sinks, the suggested heat sink was more effective in improving thermal performance. Song [13] investigated the use of case-embedded liquid cooling methods via microchannels inserted into the substrate of the electronic package for high-heat flux multi-chip arrangements. Zhang [14] developed a novel integrated cooling method for multi-chip modules by using a 3D-printed design with embedded microchannels. By using this approach, it lowers the operating temperature of high-power electronic devices and permits cooling elements to be replaced and reconfigured, allowing them to be customized for specific sources of heat and thermal demands. Ramakrishnan [15] experimentally and numerically studied using warm DI water to cool MCMs to test the performance of two heat sink designs: one with parallel channels and the other with concentrated channels. According to the findings, the cold plate with a concentrated microchannel design had superior thermohydraulic performance. Additionally, it was discovered that designing cold plates specifically for a given package is essential for achieving the best cooling results. Manaserh [16] designed a 3D-printed liquid-cooled heat sink with guiding vanes that target hotspots in high-heat flux chips using a multi-objective optimization technique. According to the study, which considers thermal and hydraulic performance parameters, the enhanced heat sink design was able to reduce hotspot temperatures by 32% when compared with the baseline design. Wadsworth [17] used a small rectangular slot to guide a two-dimensional jet of dielectric fluid into a channel that is contained between the chip surface and nozzle plate to create a correlation for the heat transfer coefficient that depends on jet width, heater length, flow velocity, and fluid properties.

In this work, an MCM experimental setup was designed and built to assess the state-of-the-art of a commercial cold plate that can be used for applications involving uniform and nonuniform heat fluxes. The experimental rig consists of four identical heaters mounted to an XYZ linear stage to give it the ability to move in three directions. A single heater test was performed as a functionality test for the experimental setup. Another test was carried out to investigate the effect of varying the coolant flow rate on the heaters' temperature and thermal resistance. A numerical model was developed to validate the experimental results, and this numerical model will be used to perform parametric studies on the microchannel design of the heat sink in future studies.

## 2. EXPERIMENTAL SETUP

An experimental rig was designed and built to replicate a real-life scenario of heterogeneous packaging of multichip modules (MCM) in high-heat flux applications, where chips and other integrated components of various heights from different manufacturers are placed closely together. This experimental rig, as seen in Fig. 1 (a) and (b), consists of four ceramic heaters, each of which has a surface area of 1.2 cm × 1.2 cm and a thickness of 0.25 cm. Each heater has a built-in K-type thermocouple near its surface to measure its temperature, and each heater can deliver a total power of 200 W with a maximum temperature limit of 400 °C. To provide precise movements in the x, y, and z directions, each heater was mounted on an XYZ linear stage. The size of the linear stage platform is 6 cm × 6 cm, and it has three knobs to control the distance in each direction. The stage is made from brass, which is a good thermal conductor. To prevent any thermal interaction that would cause heat losses between the heater and the linear stage, an insulator made from Garolite G-11 that has a low thermal conductivity of 0.288 W/m.K was placed between them. Additionally, that insulator will keep the linear stage at an appropriate temperature when the heaters are turned on, ensuring that all the heat will be transferred from the heaters to the heat sink attached to them. A commercial pin-fin heat sink, as seen in Fig. 1 (c), was used to cool the four chips, and a thermal grease thermal interface material (TIM) was applied in between.

Four separate power supplies were used, and one was connected to each heater. A liquid-to-air coolant distribution unit with a cooling capacity of 2 kW was used to control the supply fluid temperature. An external pump was used to pump DI through the loop, and the coolant flow rate was varied and controlled through an external power source connected to the pump. An ultrasonic flow meter was used to measure the coolant flow rate, and two KEYENCE GP-M001T were installed at the inlet and outlet sides to measure the pressure drop across the loop. Additionally, two T-type thermocouples were used to measure the coolant temperature at the inlet and outlet. The experimental data was gathered using a National Instruments data acquisition system (DAQ) and recorded using LABVIEW. Table 1 provides the experimental equipment's specifications.

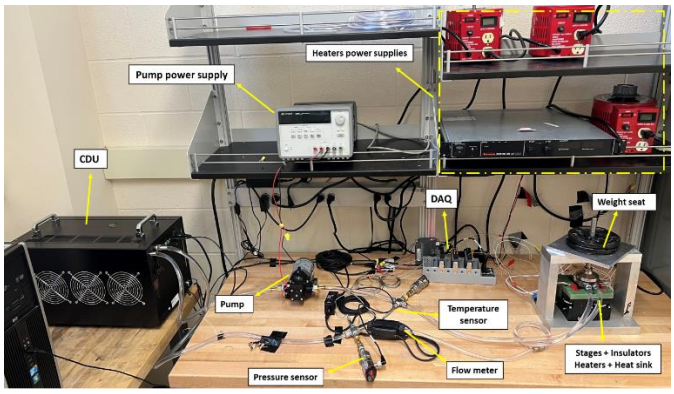


(A)

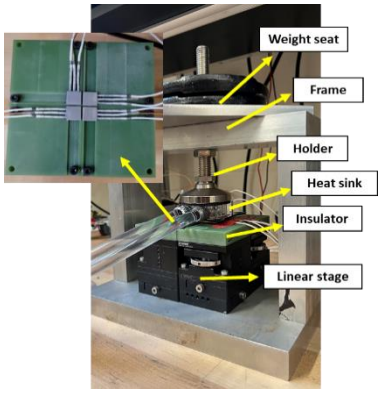


(B)

(C)

**FIGURE 1:** (A) THE EXPERIMENTAL RIG WITH ALL OF ITS COMPONENTS. (B) A MOCK PACKAGE THAT CONTAINS THE HEATERS, HEAT SINK, INSULATORS, AND STAGES. (C) THE HEAT SINK USED IN THE EXPERIMENT.

**TABLE 1:** DETAILS OF THE TEST APPARATUS.

| Apparatus | Specification |
|---|---|
| CDU | ALH-2000 (cooling capacity 2 kW) |
| Flow sensor | FD-X A1 clamp-on ultrasonic with 0.1 ml/min resolution. |
| Pressure transducer | KEYENCE GP-M001T (–100 to 100 kPa) with a resolution of (0.1 kPa) |
| Diaphragm pump | Shurflo 2088 with a maximum flow of 14 LPM |
| Insulator spacer | Garolite G-11 rated for 170 °C |
| Thermocouples | T-type (accuracy: ±0.5 ºC)<br>K-type (accuracy: ±1.1 ºC) |
| Power supplies | Sorensen DCS100-10E (1 kW output power)<br>3×VEVOR Variable Transformer (2 kW output power) |

## 3. NUMERICAL MODEL

The heat sink tested in the present study, shown in Fig. 1 (c), is composed of two parts: a plastic manifold with a single inlet and outlet and a copper base with an array of 729 square pin fins.

A Keyence VK-X1050 laser scanning microscope, a non-contact 3D surface profiler that employs laser scanning to produce high-quality pictures at high magnifications up to 100x, was used to measure the heat sink's exact geometrical dimensions. Fig. 2 depicts the microscopic images taken for the fins of the heat sink as well as their heights. Table 2 provides the heat sink's dimensions.

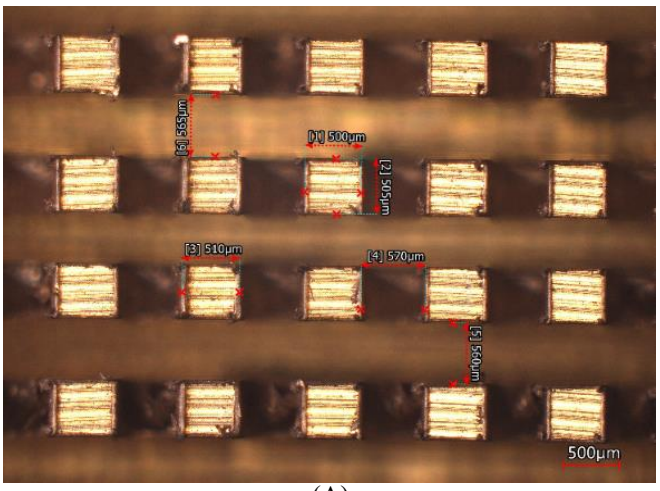


(A)

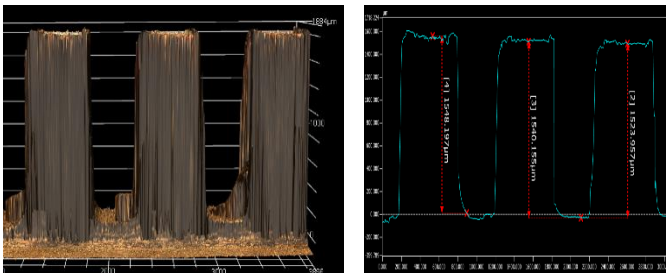

(B)

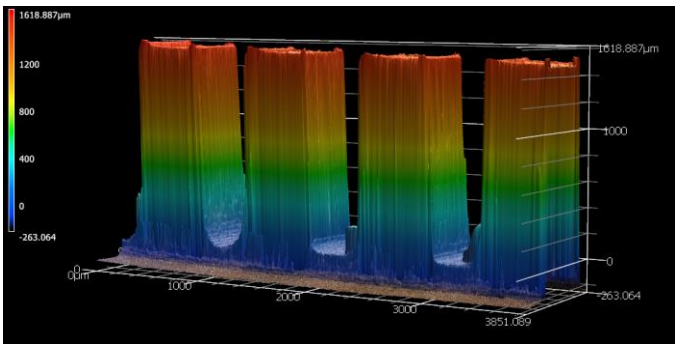


(C)

**FIGURE 2:** A MICROSCOPIC IMAGES OF THE SQUARE PIN FINS ALONG WITH A 3D GRAPHS FOR THE FIN'S HEIGHT.

**TABLE 2:** VALUES OF THE GEOMETRIC PARAMETERS OF THE HEAT SINK

| Symbol | Parameter | Value (mm) |
|---|---|---|
| $D_{in}$ | Inlet manifold port diameter | 7 |
| $D_{out}$ | Outlet manifold port diameter | 7 |
| $L$ | Base length of the heat sink | 50 |
| $W$ | Base width of the heat sink | 50 |
| $T$ | Base thickness of the heat sink | 3 |
| $h_F$ | Fin height | 1.5 |
| $w_F$ | Fin width | 0.5 |
| $w_{ch}$ | Channel width | 0.56 |

### 3.1 GOVERNING EQUATIONS AND ASSUMPTIONS

6Sigma ET was used in each simulation run for this investigation. On a staggered grid, the commercial software program discretizes and solves the system of governing equations, including the continuity, Navier-Stokes, and energy equations, employing the finite volume method. This technique is a good option for creating precise models of heat sinks for electronics since it was created expressly for modeling electronic cooling systems.

The following fundamental assumptions were used for solving the numerical models in this study:

1- The flow is 3D, steady, laminar, and incompressible.
2- No heat transfer through the surroundings, and the chips are insulated on all sides except the top, where heat transfers to the heat sink.
3- Gravity and wall roughness are negligible.
4- The effects of viscous and radiative heat transfer are insignificant.

After implementing all of the assumptions mentioned above, the continuity, momentum, and energy equations used to solve the numerical model for liquid flow and heat transfer in both fluid and solid phases are represented below:

$$\nabla \cdot \vec{u} = 0 \text{ (Continuity equation for fluid)} \quad (1)$$

$$\rho_f \left(\vec{u}.\nabla\right)\vec{u} = -\nabla P + \mu_f \nabla^2 \vec{u} \text{ (Momentum equation for fluid)} \quad (2)$$

$$\rho_f \, c_{\rho_f} \left(\vec{u}.\nabla\right) T_f = K_f \, \nabla^2 T_f \text{ (Energy equation for fluid)} \quad (3)$$

$$k_S \nabla^2 T_S = 0 \text{ (Energy equation for Solid)} \quad (4)$$

### 3.2 COMPUTATIONAL DOMAIN AND GRID STUDY

The computational domain used to conduct this investigation, which consists of the copper plate, four chips, TIM, and manifold, is depicted in Fig. 3. These components' geometries were modeled using 6SigmaET. Establishing the proper grid is essential for guaranteeing the CFD model's correctness and dependability. In this investigation, the computational domain was covered by a structured grid with hexahedral cells since it is well-known that this type of grid generation produces grids of excellent quality. The proper boundary conditions were assigned, and the grid was concentrated more in areas with high gradients.

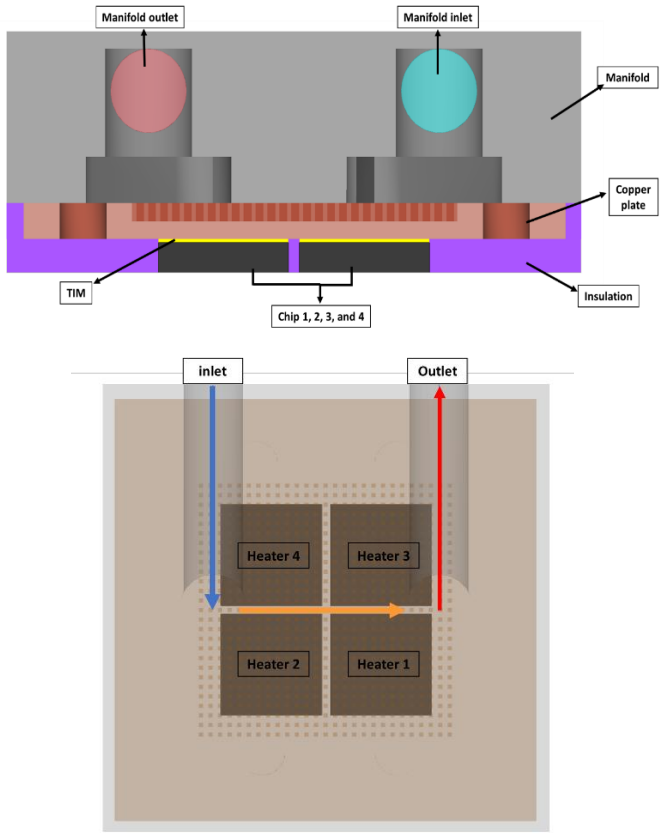


**FIGURE 3:** COMPUTATIONAL DOMAIN OF THE NUMERICAL MODEL.

During the simulation, a number of boundary conditions were used, including adiabatic and no-slip surrounding wall surfaces as well as a constant inlet flow rate. The bottom surface was an exception, as the four chips continuously produced heat. Constant pressure was assigned at the outlet. The TIM used to conduct the simulation has the same thermal characteristics as the one used in the experiment, which is Kryonaut TIM. DI water, at an inlet temperature of 32°C, served as the coolant. Table 3 lists the thermo-physical characteristics of the liquid and solid phases used in the simulation.

**TABLE 3:** THERMOPHYSICAL PROPERTIES OF FLUID AND SOLIDS.

| | ρ (kg/m$^3$) | $c_p$ (J/kg. °C) | k (W/m. °C) |
|---|---|---|---|
| Water | 995.7 | 4183 | 0.5948 |
| Copper | 8978 | 381 | 387.6 |
| Aluminum Nitride | 3260 | 780 | 160 |
| TIM | 3700 | - | 6.5 |
| Plastic | 1050 | 1670 | 0.18 |

A grid sensitivity analysis was carried out to find the optimum number of grids to guarantee correctness and consistency in the CFD model. According to the study, a grid number greater than 21 million produced only minor differences in the heat sink pressure drop and the maximum temperature for the four heaters. Fig. 4 demonstrates that increasing the number of grids from 21 to 31 × $10^6$ causes a little variation in the heat sink pressure drop and heater temperature of 0.1% and 0.4%, respectively. Therefore, the number of grids chosen was 22 million, and the smallest cell sizes were 12, 7, and 6.2 × $10^{-5}$ in the x, y, and z directions. The flow was in the laminar region for the targeted flow rates from 1 to 2 LPM where Reynolds number ranges from 720 to 1230.

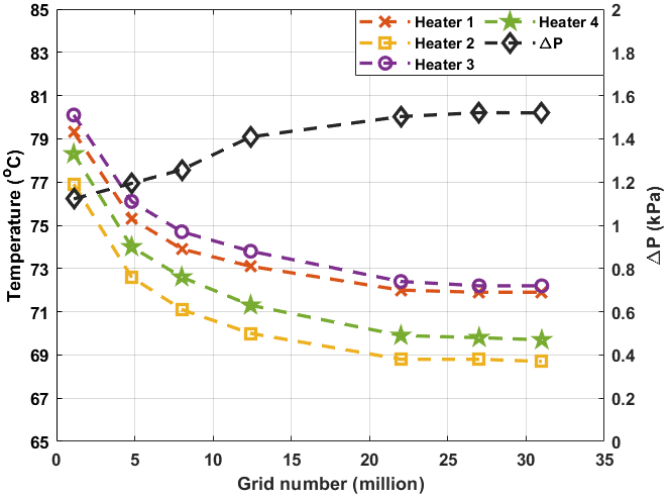


**FIGURE 4:** RESULTS OF THE GRID STUDY BASED ON THE HEATERS' TEMPERATURES AND PRESSURE DROP OF THE HEAT SINK.

## 4. PERFORMANCE METRICS

It is vital to take into account and evaluate certain response metrics, including hydraulic and thermal performance, to compare different heat sink designs. Performance can be assessed using the total thermal resistance, as seen in the schematic diagram in Fig. 5, which is calculated as the difference between the maximum chip case temperature ($T_{j,max}$) and the coolant supply temperature ($T_{coolant,in}$) divided by the total power of the electronic chips ($q_{total}$). This can be mathematically stated as follows:

$$R_{th,tot} = \frac{T_{j,max} - T_{coolant,in}}{\sum_{i=1}^{4} q_i} \quad (5)$$

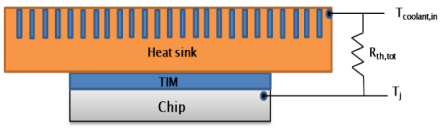


**FIGURE 5:** THERMAL RESISTANCE CIRCUIT DIAGRAM.

The below equation was used to calculate the amount of heat captured by the coolant, which indicates the amount of heat losses when compared to the power supplied by the power source.

$$q_{removal} = \dot{m}_{liq} C_{p_{liq}} \left(T_{Liq,out} - T_{Liq,in}\right) \quad (6)$$

Where $q_{removal}$ is the amount of heat picked up by the coolant, $\dot{m}_{liq}$ is the liquid mass flow rate, and $C_{p_{liq}}$ is the liquid specific heat.

## 5. RESULTS AND DISCUSSION

### 5.1 VALIDATION

The key objective is to verify the CFD modeling's accuracy so that it can be used confidently for next-level investigations and that the outcomes will be reliable for future studies. One of the experiments was used to validate the numerical model in terms of the heaters' temperature and the heat sink's pressure drop. The experiment was conducted at these boundary conditions: input power of 136 W/heater, fluid inlet temperature of 32 °C, fluid flow rate of 1 LPM, and the distance between each heater was 1 mm, and they were all at the same height. Fig. 6 compares the experimental and numerical data. The maximum discrepancy in the heaters' temperature and heat sink pressure drop between the experimental and numerical results was less than 1.4% (less than 1 °C) and 4.2%, respectively.

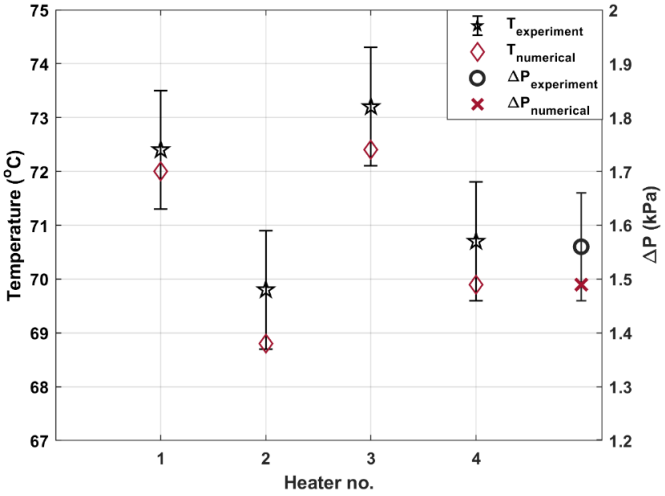


**FIGURE 6:** COMPARISON BETWEEN NUMERICAL AND EXPERIMENTAL RESULTS IN TERMS OF THE HEATERS' TEMPERATURE AND PRESSURE DROP.

### 5.2 FUNCTIONALITY TEST OF THE HEATERS

Before running any high-power tests, some preliminary tests were conducted to test the functionality of the experimental setup apparatus. The heaters' thermocouples were tested at room temperature, and the readings were found to be consistent, as seen in Fig. 7 (a). Next, another experiment was conducted by turning on one heater at the specified boundary conditions: the total input power was 163 W, the coolant flow rate was 1 LPM, and the coolant inlet temperature was 28 °C. At steady state, the

heater temperature was approximately 46.7 °C, as seen in Fig. 7 (b), and using Eq. 6, the calculated heat removal by the coolant was 160 W, which indicates the amount of heat lost in the system, which was less than 2% compared to the input power from the power supply.

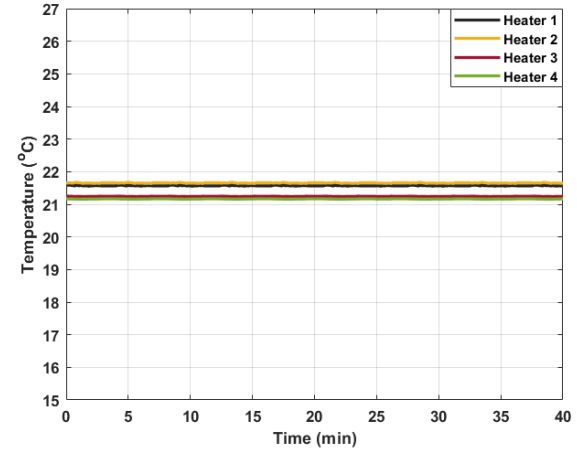


(A)

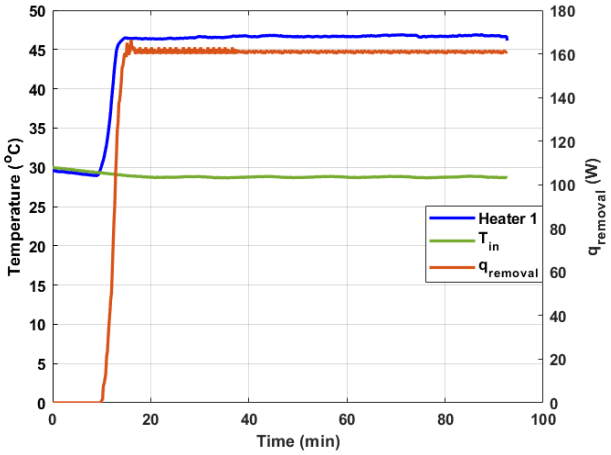


(B)

**FIGURE 7:** (A) THERMOCOUPLE READINGS AT ROOM TEMPERATURE. (B) SINGLE HEATER TEST RESULTS.

## 5.3 FOUR HEATERS TEST

The novelty of this experimental setup is to test different heat sink designs for MCM by varying multiple parameters like coolant flow rate, supply coolant temperature, uniform and nonuniform heat fluxes, and different spacings and heights between the heaters. However, only one experiment was carried out; it was performed by placing the heaters 1 mm apart, and they were all at the same height. Uniform heat flux for all the heaters, the total input power was 544.3 W (~94.5 W/cm$^2$ per heater). The supply fluid temperature was 32 °C, and the coolant flow rate varied from 1 to 2 LPM in steps of 0.25 LPM. Fig. 8 shows the heaters' case temperatures after reaching a steady state as the coolant flow rate varied. Increasing the flow rate has a big effect on the case temperatures because of the increase in the convective heat transfer coefficient. However, at a higher flow rate, the heaters' temperatures were almost the same and more uniform because the flow became more uniform in the heat sink channels, and a higher fluid velocity was observed in the channels with more fluid penetration in the heat sink microchannels, as can be seen from the streamlines and temperature contours for the four heaters in Fig. 9 (a) and (b). In Fig. 9 (b) it can be seen that there is a nonuniformity in the heaters' temperatures at 1 LPM, and when the flow rate increased to 2 LPM the temperatures are more uniform.

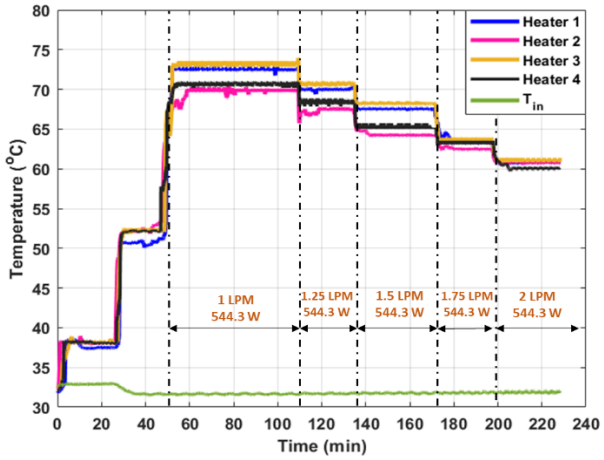


(A)

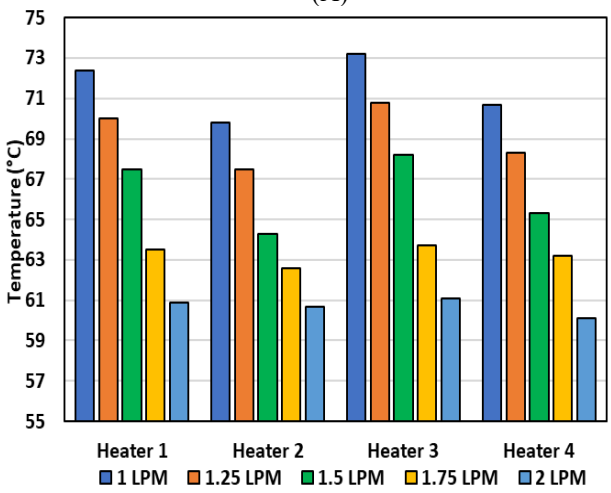


(B)

**FIGURE 8:** EFFECT OF COOLANT FLOW RATE ON THE HEATERS' CASE TEMPERATURES.

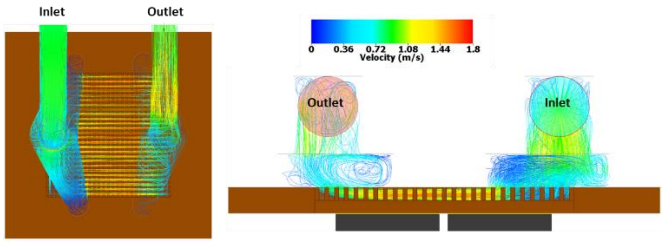


(A)

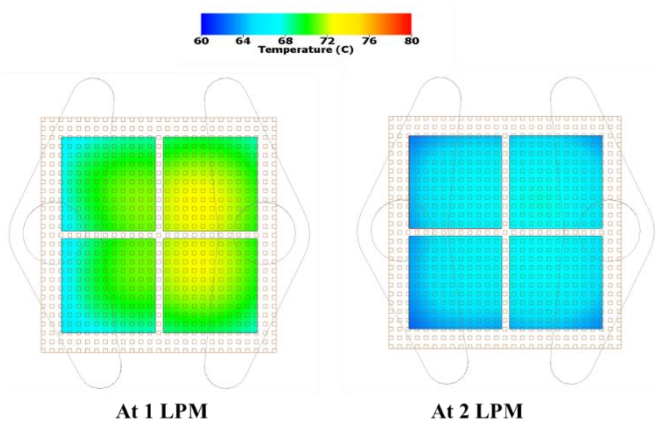


(B)

**FIGURE 9:** (A) VELOCITY STREAMLINES AT A COOLANT FLOW RATE OF 2 LPM. (B) TEMPERATURE CONTOURS FOR THE HEATERS AT 1 AND 2 LPM.

The total thermal resistance was calculated for both experiment and numerical data at different flow rates by using Eq. 5 and plotted in Fig. 10. The thermal resistance decreased by 29% because of the decrease in the liquid caloric resistance and the increase in the heat transfer coefficient. Going beyond a flow rate of 2 LPM will result in a minimal effect on thermal resistance, and any further enhancement in thermal performance becomes less noticeable.

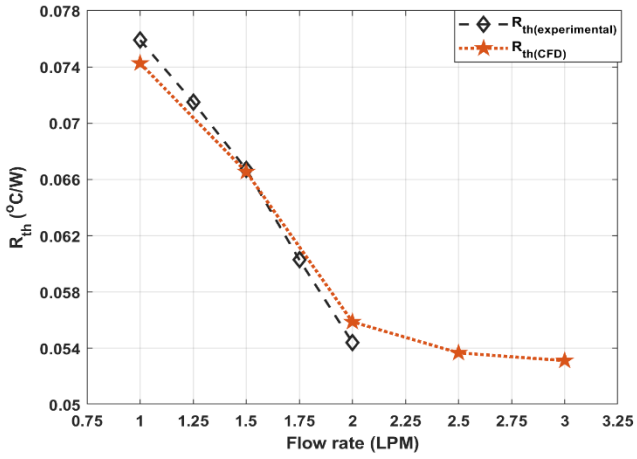


**FIGURE 10:** THERMAL RESISTANCE COMPARISON AT DIFFERENT FLOW RATES.

## 5.4 HYDRAULIC PERFORMANCE

The pressure drop across the system was measured by measuring the pressure at the inlet and outlet using KEYENCE GP-M001T pressure sensors capable of measuring in the range of -100 to 100 kPa. Before attaching the heat sink to the loop and connecting the inlet and outlet to it, the pressure drop of the system was obtained at different flow rates by looping the inlet and outlet sides together. After that, the heat sink was connected to the inlet and outlet ports, and pressure readings were taken during the experiments. By subtracting the pressure drop measurements with the heat sink attached from the pressure drop of the looping system, only the pressure drop of the heat sink was computed.

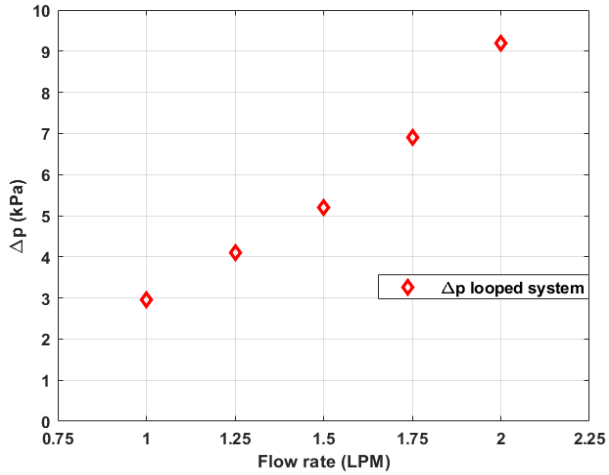


(A)

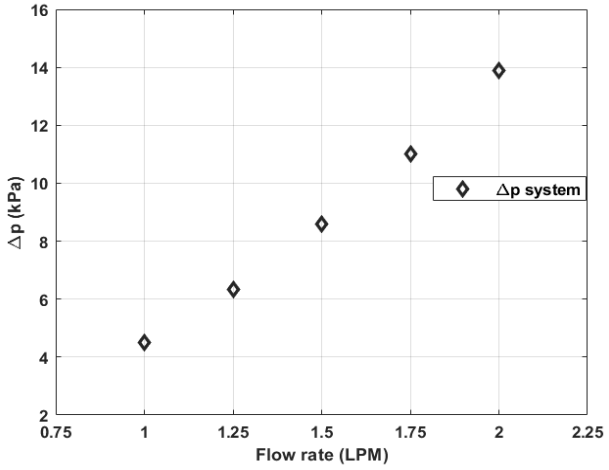


(B)

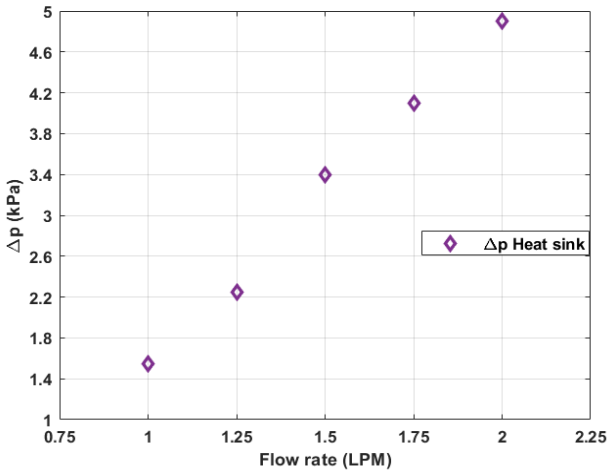


(C)

**FIGURE 11:** (A) PRESSURE DROP OF THE SYSTEM WHEN IT WAS LOOPED TOGETHER. (B) PRESSURE DROP OF THE SYSTEM INCLUDING THE HEAT SINK. (C) PRESSURE DROP OF THE HEAT SINK.

## 6. CONCLUSION

The development of MCM packaging will allow cold plates of the next generation to manage several hot spots together. Special cold plate configurations are needed for each type of packaging in order to effectively remove heat from the chips. In this work, a novel experimental setup was built to simulate a real-life scenario of MCM by using four ceramic heaters of the same size. The experimental setup was used to characterize a commercially available heat sink and observe the heaters' case temperature at constant heat flux and different flow rates. Furthermore, a numerical model was created to support the findings of the experiment. The flow rate has a big impact on thermal performance; increasing the flow rate decreased the total thermal resistance by 29% at a flow rate of 2 LPM and a pressure drop of 4.9 kPa, and at higher flow rates, the temperatures of the heaters are almost uniform and equal. However, increasing the flow rate will increase the pressure drop, which will cause an increase in the required pumping power.

## ACKNOWLEDGEMENTS

This work is supported by NSF IUCRC Award No. IIP-2209776 and MRI Award No. CNS1040666.

## REFERENCES

[1] Z. He, T. Ding, Y. Liu, and Z. Li, "Analysis of a district heating system using waste heat in a distributed cooling data center," *Appl Therm Eng*, vol. 141, pp. 1131–1140, Aug. 2018, doi: 10.1016/J.APPLTHERMALENG.2018.06.036.

[2] Y. M. Manaserh, M. I. Tradat, A. R. Gharaibeh, B. G. Sammakia, and R. Tipton, "Shifting to energy efficient hybrid cooled data centers using novel embedded floor tiles heat exchangers," *Energy Convers Manag*, vol. 247, p. 114762, Nov. 2021, doi: 10.1016/J.ENCONMAN.2021.114762.

[3] A. Shehabi, S. Smith, D. Sartor, R. Brown, and M. Herrlin, "United states data center energy usage report," 2016, Accessed: Apr. 14, 2023. [Online]. Available: https://escholarship.org/content/qt84p772fc/qt84p772fc.pdf

[4] J. Broughton, V. Smet, R. R. Tummala, and Y. K. Joshi, "Review of Thermal Packaging Technologies for Automotive Power Electronics for Traction Purposes," *Journal of Electronic Packaging, Transactions of the ASME*, vol. 140, no. 4, Dec. 2018, doi: 10.1115/1.4040828/366154.

[5] H. Y. Zhang, D. Pinjala, and P. S. Teo, "Thermal management of high power dissipation electronic packages: From air cooling to liquid cooling," *Proceedings of 5th Electronics Packaging Technology Conference, EPTC 2003*, pp. 620–625, 2003, doi: 10.1109/EPTC.2003.1271593.

[6] I. Sauciuc, G. Chrysler, R. Mahajan, and M. Szleper, "Air-cooling extension - Performance limits for processor cooling applications," *Annual IEEE Semiconductor Thermal Measurement and Management Symposium*, pp. 74–81, 2003, doi: 10.1109/STHERM.2003.1194342.

[7] D. B. Tuckerman and R. F. W. Pease, "High-Performance Heat Sinking for VLSI," *IEEE Electron Device Letters*, vol. EDL-2, no. 5, pp. 126–129, 1981, doi: 10.1109/EDL.1981.25367.

[8] P. S. Lee, S. V. Garimella, and D. Liu, "Investigation of heat transfer in rectangular microchannels," *Int J Heat Mass Transf*, vol. 48, no. 9, pp. 1688–1704, Apr. 2005, doi:10.1016/J.IJHEATMASSTRANSFER.2004.11.019.

[9] S. G. Kandlikar and A. V. Bapat, "Evaluation of Jet Impingement, Spray and Microchannel Chip Cooling Options for High Heat Flux Removal," *http://dx.doi.org/10.1080/01457630701421703*, vol. 28, no. 11, pp. 911–923, Nov. 2011, doi: 10.1080/01457630701421703.

[10] A. R. Gharaibeh, Y. M. Manaserh, M. I. Tradat, F. W. AlShatnawi, S. N. Schiffres, and B. G. Sammakia, "Using a Multi-Inlet/Outlet Manifold to Improve Heat Transfer and Flow Distribution of a Pin Fin Heat Sink," *J Electron Packag*, vol. 144, no. 3, Sep. 2022, doi: 10.1115/1.4054461.

[11] Bar-Cohen, Avram. "Thermal management of air-and liquid-cooled multichip modules." IEEE Transactions on components, hybrids, and manufacturing technology 10, no. 2 (1987): 159-175..

[12] Ansari, Danish, and Kwang-Yong Kim. "Hotspot thermal management using a microchannel-pinfin hybrid heat sink." International Journal of Thermal Sciences 134 (2018): 27-39.

[13] Song, Yunqian, Rong Fu, Chuan Chen, Qidong Wang, Meiying Su, Fengze Hou, Xiaobin Zhang, Jun Li, and Liqiang Cao. "Case-embedded cooling for high heat flux microwave multi-chip array." Applied Thermal Engineering 214 (2022): 118852.

[14] Zhang, Nan, Binbin Jiao, Yuxin Ye, Yanmei Kong, Xiangbin Du, Ruiwen Liu, Bo Cong, Lihang Yu, Shiqi Jia, and Kunpeng Jia. "Embedded cooling method with configurability and replaceability for multi-chip electronic devices." Energy Conversion and Management 253 (2022): 115124.

[15] Ramakrishnan, Bharath, Yaser Hadad, Sami Alkharabsheh, Paul R. Chiarot, Kanad Ghose, Bahgat Sammakia, Vadim Gektin, and Wang Chao. "Experimental characterization of cold plates used in cooling multi chip server modules (MCM)." In 2018 17th IEEE Intersociety Conference on Thermal and Thermomechanical Phenomena in Electronic Systems (ITherm), pp. 664-672. IEEE, 2018.

[16] Y. A. Manaserh, A. R. Gharaibeh, M. I. Tradat, S. Rangarajan, B. G. Sammakia, and H. A. Alissa, "Multi-objective optimization of 3D printed liquid cooled heat sink with guide vanes for targeting hotspots in high heat flux electronics," *Int J Heat Mass Transf*, p. 122287, Dec. 2021, doi: 10.1016/J.IJHEATMASSTRANSFER.2021.122287.

[17] D. C. Wadsworth and I. Mudawar, “Cooling of a Multichip Electronic Module by Means of Confined Two-Dimensional Jets of Dielectric Liquid,” *J Heat Transfer*, vol. 112, no. 4, pp. 891–898, Nov. 1990, doi: 10.1115/1.2910496.